

Hyperfine electro-nuclear coupling at the quantum criticality of YbCu_4Zn

S. Gabani,¹ I. Čurlik,² F. Akbar,³ M. Giovannini,³ and J.G. Sereni⁴

¹*Institute of Experimental Physics, SAS, Watsonova 47 Košice, Slovakia*

²*Faculty of Sciences, University of Prešov, 17. novembra 1, SK - 080 78 Prešov, Slovakia*

³*Department of Chemistry, University of Genova, Via Dodecaneso 31, Genova, Italy*

⁴*Low Temperature Division, CAB-CNEA, CONICET, IB-UNCuyo, 8400 Bariloche, Argentina**

(Dated: June 24, 2025)

An increasing number of Yb-based compounds fulfill the conditions for the investigation of hyperfine electro-nuclear coupling effects related to ^{171}Yb and ^{173}Yb isotopes. Among them, the lack of magnetic order down to the millikelvin range in compounds with robust localized electronic moments and their nuclear magnetism. Although reminiscences of short range magnetic interactions may be observed below 1 K, such perturbation can be dodged investigating compounds located close to a quantum critical point (QCP), where quantum fluctuations prevent the development of magnetic correlations to develop. Within the family of cubic YbCu_4M compounds ($\text{M} = \text{Ni}, \text{Au}$ and Zn), we have investigated YbCu_4Zn that shows a logarithmic temperature dependence: $C_P/T \propto \ln(T/T_Q)$ in its electronic specific heat, as predicted for a QCP. Simultaneously, no signs of RKKY interactions are detected down to 0.03 K. Due to the low Kondo temperature of its doublet ground state, the localized $4f$ electrons weakly couple with conduction electrons, allowing the coupling between nuclear and $4f$ electron moments to become relevant. However, the remainder Kondo interaction acts on the electronic hyperfine field producing a small deviation from the standard nuclear $C_N \propto 1/T^2$ dependence into a $n < 2$ power law. The expected $n = 2$ dependence is progressively recovered under applied magnetic field.

I. INTRODUCTION

1. Proximity to a QCP

The basic requirements for a system to exhibit electronuclear hyperfine coupling are: to present a robust and localized (e.g. $4f$) magnetic moment without magnetic order, and to have isotopes with non zero nuclear momentum ($\vec{I} \neq 0$). The former condition can be achieved in systems tuned close to a quantum critical point (QCP) [1] where the magnetic order phase boundary extrapolates to zero or in presence of magnetic frustration [2]. The latter condition is fulfilled e.g. by Yb^{3+} atoms whose natural concentration of $\vec{I} \neq 0$ isotopes is 14% of ^{171}Yb and 16% of ^{173}Yb [3].

The family of cubic compounds YbCu_4M ($\text{M} = \text{Ni}$ [4], Au [5]) and Zn [6] and YbNi_4N ($\text{N} = \text{Mg}$ [7] and Cd [8]) possess these characteristics. The topological conditions for magnetic frustration are provided by the fcc structure of MgCu_4Sn type (ternary derivative of the AuBe_5 -type structure) with respective lattice constants $a = 6.943 \text{ \AA}$ [4], 7.046 \AA [5, 9], 7.046 \AA [6], 7.032 \AA [7] and 6.975 \AA [8] and full occupation of the atoms in each site. This fcc lattice can be viewed as a network of edge-sharing tetrahedra with Yb magnetic ions located at the vertices, being a 3D analog of a triangular lattice [10, 11].

Although there is a larger number of YbCu_4X compounds ($\text{X} = \text{M}$ plus $\text{Cd}, \text{Ag}, \text{Tl}$ [6] and $\text{In}, \text{Ga}, \text{Pd}$ [12]) with this cubic structure, only those belonging to the M group were studied down to very low temperature. In Fig. 1 we compare the low temperature specific heat C_P/T ratio of these compounds. Two different types of $C_P/T(T)$ dependencies can be distinguished in the figure. One for $\text{M} = \text{Ni}$ and Au (note that Ni results equal those of $\text{Au}_{0.6}$, therefore not included for clarity), and the other for YbCu_4Zn .

In the case of $\text{YbCu}_{5-x}\text{Au}_x$ alloys, the decreasing transition temperature from $T_m(x) = 0.8 \text{ K}$ at $x = 1$ towards a short range interactions crossover at $T_m(x = 0.4) = 0.1 \text{ K}$ [5], extrapolates to $T_m \rightarrow 0$ for $x = 0.32$ [13]. Notably, the $T_m(x)$ anomaly seems to vanish before to reach $T_m = 0$ like many other compounds approaching a QCP from the magnetic side [15]. Coincidentally, these compounds show a power law $C_P \propto 1/T^p$ dependence above T_m which is characteristic of a spin-liquid behavior [2]. Similar behavior is observed in YbCu_4Ni ($T_m = 0.2 \text{ K}$) [4]. In the case of isoelectronic Cu and Au atoms in the $\text{YbCu}_{5-x}\text{Au}_x$ alloys

Within the $x \leq 1$ range of concentration in the $\text{YbCu}_{5-x}\text{Au}_x$ isoelectronic Cu/Au alloys, Cu substitutes the larger Au atoms in the $4c$ Wyckoff position increasing the relative available volume [16] of Yb atoms. In fact, the lattice parameter decreases less than the extrapolation following the Vegards law from higher Au concentrations [14]. Then, is the decrease of Au con-

* jsereni@yahoo.com

$= A_{hf}(\hat{J}^*\hat{I})$, and iv) nuclear-dipolar interaction: $H_{dip} = A_{dip}(\hat{I}^*\hat{I})$. The former, H_R , induces long range magnetic order that inhibits the ‘ hf ’ interaction, and the last is quite weak compared with the other interactions. Quadrupolar interaction is not considered here because of the lack of electric gradient in the cubic crystallographic symmetry of the investigated compounds [27].

The effective magnetic field induced by the localized $4f$ electrons on the nuclear magnetic moments ($\mu_I = g_I \mu_n \vec{I}$) may reach hundreds of Tesla, that splits the \vec{I} degenerated levels producing a low temperature Schottky anomaly in the nuclear specific heat $C_N(T)$.

Therefore, this work is mainly devoted to the study of the competition between H_K and H_{hf} scales of energy because the former interaction triggers a fast relaxation mechanism ($\tau = \hbar/k_B T_K$) that prevent the slower nuclear-electron relaxation [13].

II. EXPERIMENTAL RESULTS

A. Specific heat

Going back to Fig. 1, the measured $C_P/T(T)$ of the three isotypic Yb-compounds can be better analyzed after defining two regions: the ‘‘paramagnetic’’ (for $T > 0.1$ K), and the ‘‘nuclear’’ one (for $T < 0.1$ K), where the $C_N/T(T)$ component grows above the paramagnetic $C_{4f}/T(T)$ contribution. In the former, one can appreciate that the compounds belonging to the ‘magnetic’ side of the QCP follow a power law dependence: $C_P/T(T) \propto 1/T^p$, with an exponent $p = 1.4$ for YbCu₄Ni [4], that progressively decreases to $p = 0.9$ for YbCu_{4.5}Au_{0.5} [5] and to $p = 0.75$ for YbCu_{4.6}Au_{0.4} [13]. This confirms that YbCu_{5-x}Au_x approaches to a QCP from the magnetic side as Au concentration decreases.

Notably, the specific heat anomalies at $T = T_m$ of YbCu₄Ni and YbCu_{5-x}Au_x look like different stages in the evolution of the same type of magnetic crossover. In fact, the curve corresponding to YbCu_{4.4}Au_{0.6} is not included in Fig. 1 for clarity because it coincides with that of YbCu₄Ni.

As mentioned before, a completely different behavior of $C_P(T)/T$ is observed for YbCu₄Zn, that corresponds to a logarithmic temperature dependence, as it is expected for non-fermi-liquid (NFL) systems [19]. This compound is therefore placed into the ‘non-magnetic’ side of the QCP (see Fig. 2) because there are no traces of magnetic interactions, even under applied magnetic field of $B = 9$ T. The $\log(T/T_0)$ dependence is discussed in the next subsection devoted to the data presented in Fig. 3a.

The comparison of the $C_P(T)/T$ dependencies of these compounds offers a unique opportunity to gain insight into the thermodynamic behavior of magnetic

systems in the vicinity of a QCP because their isotypic and isostructural character. As it is presented in Fig. 1, the T dependencies in the paramagnetic region indicates to which side of the QCP belongs the system. Following the decreasing evolution of the p exponent of $C_P(T)/T \propto 1/T^p$, one notes that this function tends to $\log(T/T_0)$ for very low p values. We remark that the studied YbCu_{5-x}Au_x alloys with $p = 0.9$ and 0.75 are exceptional cases of $p \leq 1$ exponents which allow to speculate on the lack of a discontinuity undergoing a QCP because of the presence of quantum fluctuations. Therefore, the definition for a QCP as the limit of a second order transition extrapolation to zero [1] does not occur in real systems because their magnetic phase boundaries transform from well defined phase-transition into some type of ‘crossover’ (at $T = T_m$) as the quantum fluctuations become dominant. Interestingly, in Fig. 1 one can see that the degrees of freedom associated to the crossover vanish faster than $T_m \rightarrow 0$. This means that in this case quantum fluctuations blur the crossover preventing T_m to reach $T = 0$ as mentioned for other systems [15].

Concomitant with the vicinity to a QCP and the consequent lack of magnetic order both, YbCu_{4.6}Au_{0.4} alloy and stoichiometric YbCu₄Zn, clearly exhibit the arising nuclear contributions $C_N(T)/T$ below about 0.1 K. Notably, in both cases $C_N(T)$ does not show the expected $C_N/T \approx \alpha/T^3$ dependence [17] for well defined nuclear levels. Instead, a $\alpha_n/T^{2+\epsilon}$ dependence is observed, as indicated on the low temperature side of Fig. 1. The origin of this deviation is discussed in Section IV.

1. Analysis of the YbCu₄Zn results

At low temperature, the logarithmic $C_m(T)$ behavior of YbCu₄Zn is demonstrated in Fig. 3a in a $C_m/T \propto \log(T/T_Q)$ representation, where the characteristic temperature: T_Q , is a scale of energy for the quantum fluctuations. For this figure three ranges of specific heat measurements are matched: i) the very low temperature: $0.05 \geq T \geq 1$ K, measured in a dilution refrigerator, ii) the low temperature $1 \geq T \geq 8$ K measured in a PPMS devise (Quantum Design) and iii) the intermediate temperature $T \geq 8$ K extracted from Ref. [6] after the C_{ph} subtraction. The low $T_Q = 6$ K value, obtained from the fit in Fig. 3a, indicates the vicinity of this compound to the QCP.

The NFL character of the $C_m(T)$ behavior of YbCu₄Zn can be verified using the universal scaling criterion for NFL systems: $C_m/t = -D \log(t) + ET_0$ [20], as shown in Fig. 3b. There, $t = T/T_0$ and $D = -7.2$ J/molK. Since D is fixed, T_0 is the only free parameter that provides an energy scale compar-

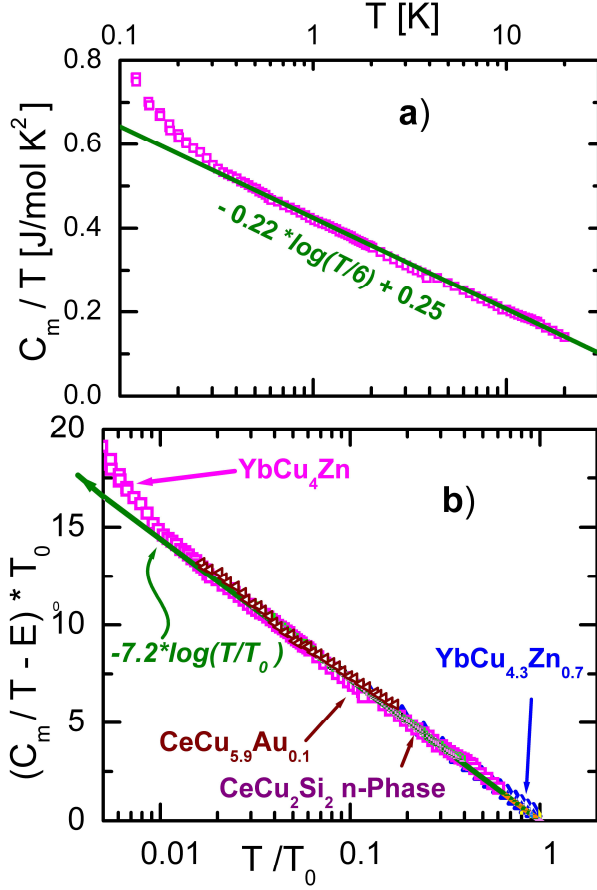


FIG. 3. (Color online) a) Logarithmic temperature dependence of YbCu₄Zn. b) Comparison of different NFL compounds within the normalized procedure (see text).

ison between different systems. E accounts for the conduction band contribution. For YbCu₄Zn one obtains $T_0 = 33$ K and $E = 90$ mJ/mol K², that can be contrasted with CeCu_{5.9}Au_{0.1} [21]: $T_0 = 5.3$ K and $E = 53$ mJ/Kmol, and the n-phase of CeCu₂Si₂ [22]: $T_0 = 14$ K and $E = 40$ mJ/Kmol. Also for comparison, the Cu-rich alloy YbCu_{4.3}Zn_{0.7} alloy [24] is included in the figure with $T_0 = 16$ K and $E = 170$ mJ/Kmol, suggesting to be closer to the QCP than the isotypic stoichiometric compound. In fact the standard $C_m(T)/T$ values measured above 2 K are about 50% larger than those of YbCu₄Zn.

Although the $C_m/T \propto \log(T/T_Q)$ dependence of YbCu₄Zn appears as an exception within this family of compounds, it is not an exception because by 19% of Sc substitution in Yb_{1-x}Sc_xCo₂Zn₂₀ this compound also shows a $\log(T/T_Q)$ dependence approaching a QCP [23].

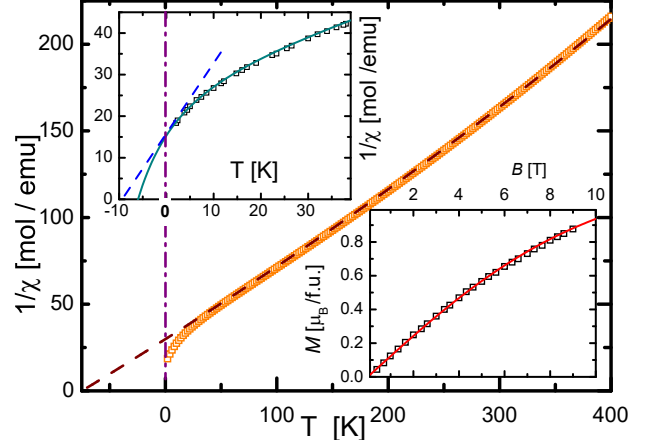


FIG. 4. (Color online) Inverse magnetic susceptibility of YbCu₄Zn measured at $B = 1$ T. Upper inset: detail at low temperature. Lower inset: Magnetization curve up to $B = 9$ T at $T = 2$ K. The continuous curve is the fit with a Brillouin function $B_{1/2}(y)$, see the text.

B. Magnetic susceptibility

The high temperature ($T \geq 50$ K) inverse susceptibility of YbCu₄Zn is presented in Fig. 4. This measurement allows to determine an effective magnetic moment $\mu_{eff} = 4.47\mu_B$ (close to the theoretic value $4.54\mu_B$ for $\tilde{J} = 7/2, \tilde{S} = 1/2, \tilde{L} = 3$ with $g_J = 1.14$) and a paramagnetic temperature $\theta_P = -70$ K. From the relation $T_K = \theta_P/\sqrt{2}$ [25] for the Kondo temperature evaluation, one extracts for high temperature $T_K^{HT} = 50$ K that include the contribution of the excited CEF levels.

High temperature specific heat measurements suggests the lowest CEF split is between two doublets with a gap of $\Delta_1 = 35$ K and therefore the $T \leq 30$ K curvature of $1/\chi(T)$ in Fig. 4 is expected to be related to the depopulation of the excited levels. In order to extract more information about the magnetic properties of the GS, we have fit the $1/\chi(T)$ dependence in the $T \leq 30$ K range s presented in the upper inset of Fig. 4. The continuous curve fits the experimental data using the function:

$$1/\chi(T) = (T + 6)/\sum_{i=0}^{i=2} a_i e^{-\Delta_i/(T+\theta_i)} \quad (1)$$

where: $a_0 = 0.03$, $a_1 = 0.72$, $a_2 = 1.94$, $\Delta_1 = 40 \pm 5$ K is close to the first CEF splitting and $\Delta_2 = 90 \pm 15$ K the energy of the quarted Γ_8 , with $\theta_1 = 25$ K and $\theta_2 = 41$ K as respective paramagnetic temperatures usually proportional to their Kondo scales. A $\theta_{GS} = -8.5 \pm 0.5$ K is obtained for the GS as a linear extrapolation to $1/\chi = 0$ from $T = 0$, i.e. following the tangent at $1/\chi(T = 0)$ From this fit one can extract the relevant parameter $T_K = \theta_{GS}/\sqrt{2} = 6 \pm 0.3$ K, which confirms

the low Kondo scale of the GS and, from the slope of the $1/\chi(T=0)$ extrapolation, a $\mu_{eff}(GS) = 2.13\mu_B$ is extracted.

C. Magnetization

In the lower inset of Fig. 4 we show the field dependent magnetization $M(B)$ measured at 2 K. The experimental curve is properly fitted with a Brillouin function $B_{1/2}(y)$ (continuous curve), where $y = g_{eff}\mu_B JB/k_B T$ and $g_{eff} = 0.6$ for the present doublet GS. This function is normalized to a saturation value of $M_{sat} = 1.23\mu_B$. Comparing this saturation value with the values for the two possible GS doublets: $M_{sat}(\Gamma_6) = 1.33\mu_B$ and $M_{sat}(\Gamma_7) = 1.72\mu_B$, it is evident that Γ_6 is the most likely GS. Furthermore $\mu_{eff}(GS)/M_{sat}(2 K) = 2.13\mu_B/1.23\mu_B = \sqrt{3}$.

III. DISCUSSION

Once established that YbCu₄Zn is a compound placed on the "non-magnetic" side of a QCP, we can analyze the unexpected exponent of the power law increase of $C_P/T(T)$ below $T = 0.1$ K, mentioned in Fig. 1 within the context of the interaction between the localized $4f$ electrons and nuclear spins.

From the comparison with the other isostructural compounds symmetrically placed on the "magnetic" side of the QCP one sees that: i) the so called Kondo interaction between local and band electrons (T_K) is present on both sides of the QCP, ii) its energy scale is quite similar, concomitant with their similar electronic configurations and crystalline structures, and therefore: iii) there are no indications that $T_K \rightarrow 0$ at the QCP as it might be expected from theory, though the observed values are quite low and equivalent to those of quantum fluctuations.

The question arises how these fluctuations: remnant of Kondo or quantum fluctuations, affect the interaction between local electrons and nuclear moments. For such a purpose we have studied the field dependence of the specific heat of YbCu₄Zn at very low temperature and analyzed its evolution in the context of the hyperfine interaction. blundell

A. Hyperfine coupling

The dipole hyperfine coupling energy: $H_{hf} = A_{hf}(\vec{I} \cdot \vec{J})$, where A_{hf} is the hyperfine constant, arises from the interaction between the nuclear \vec{I} and the electronic moments \vec{J} .

The element Yb (atomic number 70) possesses a number of stable isotopes [26]. Those with even mass, from 170 to 176 and total abundance of $\approx 70\%$, have zero nuclear moment $\vec{I} = 0$. The most relevant Yb isotopes with odd mass (171, 173) and $\vec{I} \neq 0$ nuclear moment have an abundance: 14 % ^{171}Yb with $\vec{I} = 1/2$ and 16 % ^{173}Yb with $\vec{I} = 5/2$ respectively.

Therefore, only the $\approx 30\%$ isotopes with $\vec{I} \neq 0$ are involved into the hyperfine coupling. As a consequence, the electronic magnetic properties acting on all Yb atoms in the paramagnetic region, is reduced to 1/3 of the atoms regarding the nuclear contribution observed at $T \leq 0.1$ K. This suggests that in the study of that contribution, the original chemical formula of YbCu₄Zn can be reformulated for practical reason as: $(0.7 \text{ } ^{170}\text{Yb} + 0.14 \text{ } ^{171}\text{Yb} + 0.16 \text{ } ^{173}\text{Yb})\text{Cu}_4\text{Zn}$ below ≈ 0.1 K. Thus, only the 30% of the sample: $0.14 \text{ } ^{171}\text{Yb} + 0.16 \text{ } ^{173}\text{Yb})\text{Cu}_4\text{Zn}$ is involved in the hyperfine interaction.

The total angular moment originated in the combination of nuclear and electron moments ($H_{hf} = A_{hf}(\vec{I} * \vec{J})$), is given by: $\vec{F} = \vec{I} + \vec{J}$ [28], with the possible hyperfine couplings for each isotope: i) ^{171}Yb , with $\vec{I} = 1/2$ and $\vec{J} = 1/2 \Rightarrow \vec{F} = 0$ and 1, and ii) ^{173}Yb , with $\vec{I} = 5/2$ and $\vec{J} = 1/2 \Rightarrow \vec{F} = 2$ and 3. The former case reminds the ortho-para nuclear spin order in Hydrogen molecules and magnetic dimers formation [28]. We notice that in the isotropic cubic crystalline symmetry of YbCu₄Zn, the nuclear Quadrupolar Gradients can be neglected [27].

B. Nuclear contribution to specific heat

In order to elucidate which one of the two contributions, from ^{171}Yb or from ^{173}Yb , is the relevant in this case one can take as a reference the studies performed on diluted ^{171}Yb into the cubic-fcc matrix Au [27].

In Fig. 5, the nuclear contribution to the specific heat of ^{171}Yb : $C_N = C_{meas} - C_{Au}$, after [27] is presented. Red curve: Schottky like fit with upper inset (red) level scheme: $\vec{F} = \vec{I} \pm \vec{J} = 1$ and 0, with $\vec{I} = 1/2$ and $\vec{J} = 1/2$, and $A_S > 0$. From this fit the 'hf' factor $A_{1/2}(171) = 130$ mK was extracted. Notice that in this configuration the GS is the singlet $\vec{F}_0 = 0$, while the excited state is the triplet $\vec{F}_1 = 1$.

For comparison, the blue Schottky curve corresponds to the lower inset (blue) level scheme: $\vec{F} = \vec{I} \pm \vec{J} = 2$ and 3 with $\vec{I} = 5/2$ and $\vec{J} = 1/2$, and $A_{5/2}(173) = 35$ mK. There one can appreciate the difference in temperature and height of the maximum. It is evident that the involved entropies are quite different in both energy schemes: with $\Delta S_1 = R \ln(4)$ for

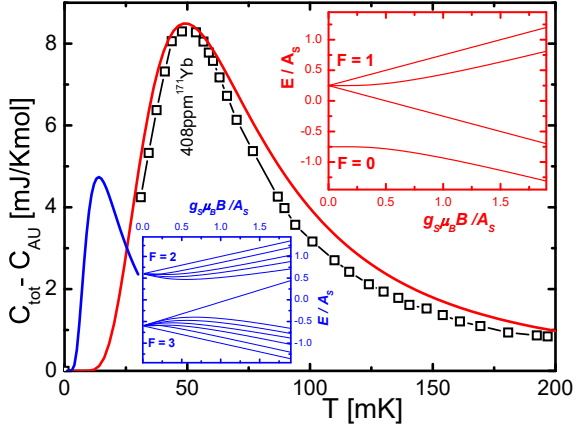


FIG. 5. (Color online) Nuclear contribution to specific heat of ^{171}Yb diluted in AuYb after [27] (open squares). Red curve: Schottky anomaly fit following the energy levels scheme presented in the upper (red) inset, with $\vec{F} = \vec{I} \pm \vec{J} = 1$ and 0 , from $I = 1/2$ and $J = 1/2$, and $A_S > 0$. Blue curve: Schottky anomaly fit following the lower inset (blue) energy levels scheme, with $\vec{F} = \vec{I} \pm \vec{J} = 2, 3$ from $I = 5/2$ and $J = 1/2$, and $A_{hf} < 0$.

$\vec{F}_0 \rightarrow \vec{F}_1$, and $\Delta S_2 = R \ln(12/7)$ for $\vec{F}_3 \rightarrow \vec{F}_2$, even though the $A_{5/2}$ contribution is not negligible. However, for practical reasons, we will refer all the measured $C_N(T)$ contribution to the $A_{1/2}$ coupling scheme because it is the dominant one within our experimental range of temperature: $T \geq 50$ mK.

1. The case of YbCu_4Zn

Paying attention, once again, to the $T \leq 0.1$ K side of Fig. 1, we have remarked that —the C_P/T measurements on YbCu_4Zn and $\text{YbCu}_{4.6}\text{Au}_{0.4}$ are compared with a $C_N/T \propto 1/T^2$ dependence and not with the expected $C_N(T)/T \propto 1/T^3$, which corresponds to the high temperature limit of a Schottky type anomaly describing the split of nuclear levels produced by the effective field B_{eff} arising from the orbiting $4f$ electrons [17]. In fact, as it is shown in Fig. 5 for AuYb , the nuclear contribution is properly described by a Schottky anomaly with a $C_N \propto \alpha_n/T^2$ high temperature tail. Due to the limited range in which this temperature dependence is measured, the exponent $n = 2$ has to be taken as an approximation reference. Nevertheless, it is far from the expected value $n = 3$. In order to reduce this uncertainty, we have also studied the $C_N(T)$ evolution as a function of field, presented in Fig. 6a as $C_P(T, B)/T$ for $0 \leq B \leq 8$ T. There one can appreciate that neither for the highest applied field the $\propto 1/T^3$

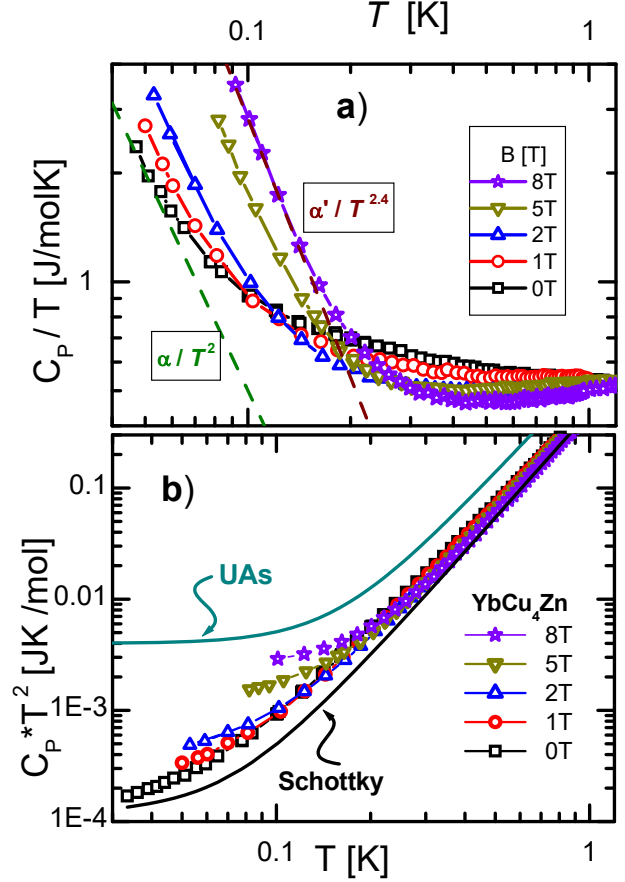


FIG. 6. (Color online) a) Low temperature specific heat of YbCu_4Zn divided temperature remarking the nuclear $C_N(T)$ contribution. Green and brown lines indicate the different exponent of thermal dependence: C_N/T^n , for $B = 0$ and $B = 8$ T respectively. b) $C_P * T^2$ representation evidencing the exponent variation with field (see text). Continuous (black) curve is the Schottky anomaly better approaching the behavior for $B = 0$. The dark-cyan curve represents the Schottky like behavior of UAs [29] as a reference of a system with C_N/T^2 . Note that in the figure the total measured specific heat C_P/T is represented, that includes phonon and electronic band contributions in double logarithmic scale.

dependence is reached.

The total measured signal includes nuclear, electronic band and phonon contributions: $C_P/T = C_N/T + C_{el}/T + C_{phon}/T = \alpha/T^3 + \gamma + \beta * T^2$, with a negligible contribution of the $\beta * T^2$ term in the $T < 1$ K range. Two reference (dashed) lines are included in the figure, one for the $B = 0$ measurement as α_n/T^2 (green) and the second as $\alpha_n^*/T^{2.4}$ for $B = 8$ T (brown). Note that the fit for $B = 0$ is affected by a significant error (around 15%) because of the few points involved. Nevertheless, the relevant physics concerns the clear difference with

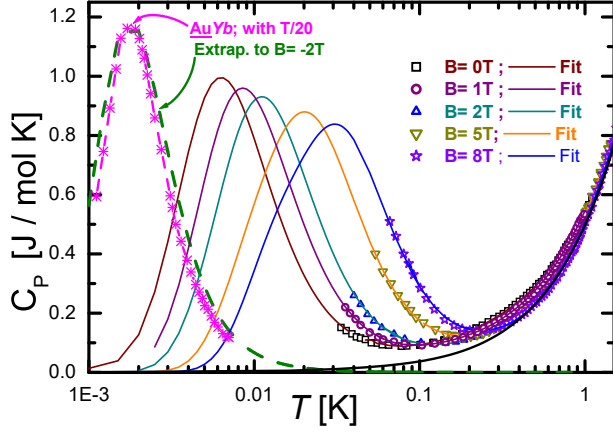


FIG. 7. (Color online) Fits of the specific heat using Schottky anomalies in a semilogarithmic representation, that accounts for the excitation from the singlet GS \vec{F}_0 to the triplet \vec{F}_1 . A level broadening for the upper level (see text) and the electronic contribution: $\gamma * T$ are included. Green dashed curve is the reference for the $\gamma * T$ contribution. Magenta dashed curve represents the $C_P(T)$ of AuYb after [27] with $T_{max}/10$, which is included as reference.

the expected $\propto 1/T^3$ dependence, and the variation of that exponent increasing the magnetic field.

In order to make more evident the previously discussed change of the exponent we represent in Fig. 6b the temperature dependence of the specific heat as: $C_P * T^2 = \alpha_n + \gamma * T^3$ to better visualize the deviation from the high temperature tail of the Schottky anomaly. The $C_P * T^2$ extrapolation to $T \rightarrow 0$ ranges between 2×10^{-4} for $B = 0$ and 3×10^{-3} JK/mol for $B = 8$ T. These values are compared with those of UAs [29] (black curve) included into the figure as reference and an 'ad hoc' Schottky anomaly. Both references were chosen because they show respective $C_N \propto 1/T^2$ dependencies in a similar range of temperature like YbCu₄Zn and, consequently, a temperature independent $C_N * T^2$ contribution at $T \rightarrow 0$.

In addition to the increase of the nuclear coefficient $\alpha_n(B)$ with field, in the figure one can appreciate how the $C_P * T^2$ data evolves from a clearly different curvature compared to the Schottky anomaly at $B = 0$ towards that of the reference UAs shape for the $B = 8$ T. One might claim from Fig. 6b that at $B = 0$ the $\lim_{T \rightarrow 0}$ of $C_N * T^2$ tends to a constant α_0 , however the high temperature $T \gg \Delta$ dependence of a pure Schottky anomaly (Δ = level splitting) starts to deviate from $C_N \propto 1/T^2$ around $T = \Delta$ with the onset of a negative curvature. That range of temperature is reached at higher field measurements, without showing such curvature.

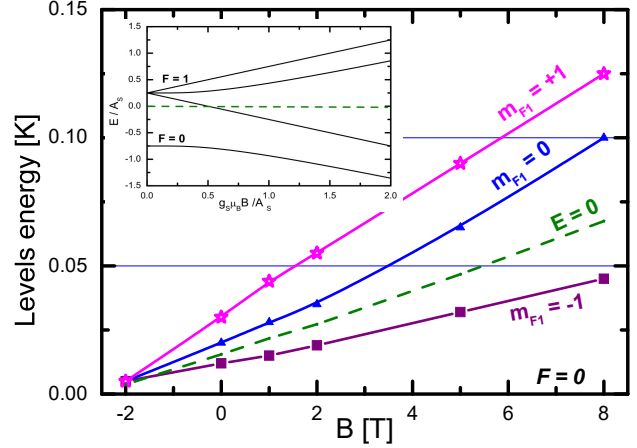


FIG. 8. (Color online) Energy variation of the \vec{F}_1 (triplet) levels by magnetic field, measured from the \vec{F}_0 (singlet) GS. Green dashed line: baricenter of energy of the full system (E_0). Inset: theoretic evaluation of the single-triplet system as a function of field, taking as reference the energy baricenter E_0 .

To gain insight into the origin of this unexpected variation of the exponent $n(B)$ in $C_N \propto 1/T^n$, we have fitted the $C_P(T)$ data with a Schottky anomaly that represents the excitation from the GS \vec{F}_0 (singlet) to the excited state \vec{F}_1 (triplet). To properly describe the experimental results, we have introduced a correction to the standard 'hf' interaction, which is based on the hypothesis that a broadening of the electronic levels is produced by a weak remnant electronic Kondo effect, which is reflected in the hyperfine effective field as a small dispersion in the energy levels. To that purpose, the upper nuclear level broadening of the \vec{F}_1 (triplet) was modeled using a Lorentian function instead of Dirac one.

For this analysis of the nuclear contribution we have considered that one Formula Units contains 0.14 ^{171}Yb isotope. These fits to $C_P(T, B)$ are shown in Fig. 7 from $B = 0$ up to 8 T, including respective electronic contributions: $\gamma * T$, which is described by the green dashed curve. Also for comparison, the $C_P(T)$ of AuYb after [27] is included, with a scaling of its by $T_{max}/10$, see magenta dashed curve.

The level energies of the excited triplet with projections: $m_{\vec{F}_1} = +1$, $m_{\vec{F}_1} = 0$ and $m_{\vec{F}_1} = -1$, are presented in Fig. 8 as a function of field. The zero energy reference corresponds to the singlet-GS \vec{F}_0 . The green dashed line indicates the energy variation of the baricenter (E_0) of the full set of nuclear levels. Note that the m_{F1} levels are already split at $B = 0$ by an internal H_{hf} field. The convergence of those levels, i.e. $H_{hf}=0$ occurs at $B = -2$ T. The theoretic evaluation of

the single-triplet sytem as a function of field is included for comparison in the inset, where the baricenter of the energy: $E = 0$, is taken as energy reference.

Since the range of temperature of the measured specific heat only covers the upper tail of the Schottky anomaly, for practical reasons only the broadening (δm) of the highest energy level: $m_{F1} = +1$, of the \vec{F}_1 (triplet) was computed to fit the $C_P(T, B)$ curves shown in Fig. 7. Within the statistical error of these fits we consider that this upper level contains the most relevant information related to the physics under study. The computed value is: $\delta m_{+1} = 25 \pm 5$ mK, which slightly decreases with increasing field.

The energy related to the broadening of the nuclear level: $\delta m_{+1} = 25 \pm 2$ mK, can be compared with the Kondo temperature: $T_K = 6.1$ K, of the electronic GS in terms of the effective fields: $H_{T_K} = k_B T_K / g_{eff} \mu_B$ and $H_{\delta m} = k_B \delta m / g_N \mu_N$ respectively. Where $g_{eff} = 0.6$ as it was evaluated from $MvsB$ at 2 K in the lower inset of Fig. 4, and $g_N = 3.34$ taken from AuYb [30], being $g_{eff}/g_N = 0.6/3.34 = 0.17$ and $\mu_B/\mu_N = 1836$. Thus, the ratio: $H_{T_K}/H_{\delta m} = (k_B T_K / g_{eff} \mu_B) / (k_B \delta m / g_N \mu_N) = (6.1/0.025)/(0.17*1836) = 0.78$, indicates coincident values within the approximations introduced in this evaluation.

Therefore, the deviation from the expected $C_N \propto 1/T^2$ dependence can be attributed to the effect of the Kondo interaction on the effective electronic field perceived by the nuclear levels.

IV. CONCLUSIONS

We have confirmed that YbCu_4Zn is tuned very close to a QCP after its NFL behavior of $C_m/T \propto -\log(T/T_Q)$ dependence and the low values of the characteristic energies extracted from thermal and magnetic

properties like: quantum fluctuations $T_Q = 6$ K and Kondo temperature $T_K^{GS} = \theta_P/\sqrt{2} = 6.1$ K.

From the comparison of respective physical properties of the YbCu_4M (M= Ni, Au and Zn) family and the isotopic YbNi_4Mg , one observes that some properties, e.g. $\chi(T \rightarrow 0)$, are similar on both sides of the QCP. However, a clear difference appears in the $C_P(T)$ between power laws and logarithmic ones. This reveals that, though the energy scales are similar, the excitation spectrum is clearly different. This set of six compounds does not prove a general behavior, nevertheless to our knowledge it is the largest group of isotopic compounds tuned in the vicinity of a QCP.

The relevant coupled hyperfine states are $\vec{F} = \vec{I} \pm \vec{S} = 0$ and 1 according to nuclear $\vec{I} = 1/2$ and electronic $\vec{J} = 1/2$, with the \vec{F}_0 singlet as a GS and \vec{F}_1 triplet as excited state. Nevertheless, the \vec{F}_1 triplet is already split at $B = 0$ by an hyperfine field $H_{hf} \approx 2$ T. The field effect induces a Zeeman-like increase of A_{hf} from ≈ 25 mK at $B = 0$ to ≈ 130 mK for $B = 8$ T

Notably, the nuclear contribution of YbCu_4Zn : $C_N(T, B) = 1/T^n$ does not obey the expected $n = 2$ dependence but a fraction with $1 \leq n \leq 1.4$ for $0 < B < 8$ T. Therefore the fits of $C_N(T, B)$ require to account for a nuclear levels broadening of ≈ 5 mK. This indicates that the Kondo mechanisms acting on the $4f$ electrons is reflected in the hyperfine coupling producing a concomitant energy widening of the nuclear levels.

The weakness of this analysis is the short range of temperature within which the $C_N(T, B)$ fit can be performed, however the physical description is strengthened by using the same fitting formula for 5 different magnetic fields. Independently of the significant indeterminacy in the value of the exponent n , the relevant information corresponds to its variation with field, that tends to the expected value $n = 2$ once the electronic Kondo effect is quenched by the applied magnetic field.

-
- [1] see for example: M. Vojta, *Quantum phase transitions*, Rep. Prog. Phys. **66** (2003) 2069–2110.
 - [2] L. Balents; *Spin liquids in frustrated magnets*; Nature **464** (2010) 199-208.
 - [3] G. Frossati, J.M. Mignot, D. Thoulouse, R. Tournier; *Van Vleck-like electronuclear susceptibility of ^{171}Yb in Au at very low temperature*; Phys. Rev. Lett. **36** (1976) 203.
 - [4] J.G. Sereni, I. Čurlík, M. Giovannini, A. Strydom, M. Reiffers, *Physical properties of the very heavy fermion YbCu_4Ni* ; Phys. Rev. B **98** (2018) 094420.
 - [5] I. Čurlík, M. Giovannini, J. G. Sereni; *Extremely high density of magnetic excitations at $T = 0$ in $\text{YbCu}_{5-x}\text{Au}_x$* , Phys. Rev. B **90** (2014).
 - [6] J. L. Sarrao, C. D. Immer, Z. Fisk, C. H. Booth, E. Figueroa, J. M. Lawrence, R. Modler, A. L. Cornelius, M. F. Hundley, G. H. Kwei, J. D. Thompson, F. Bridges, *Physical properties of YbXCu_4X (X= Ag, Au, Cd, Mg, Tl, and Zn) compounds*, Phys. Rev. B **59** (1999) 6855.
 - [7] S. Linsinger, M. Eul, C. Schwickert, R. Decourt, B. Chevalier, Ute Ch. Rodewald, J-L. Bobet, R. Pöttgen, *Structure, homogeneity ranges, magnetic, and electrical properties of the ordered Laves phases RENi_4Mg with MgCu_4Sn type structure*, Intermetallics **19** (2011) 1579-1585.
 - [8] J. Lee, H. Park, N.R. Lee-Hone, D.M. Broum, E. Mun, *Thermodynamic and transport properties of YbNi_4Cd* ,

- Phys. Rev. B **97** (2018) 195144.
- [9] E. Bauer, E. Gratz, R. Hauser, Le Tuan, A. Galatanu, A. Kottar, H. Michor, W. Perthold, G. Hilscher, T. Kagayama, G. Oomi, N. Ichimiya and S. Endo, *Pressure- and field- dependent behavior of YbCu_4Au* , Phys. Rev. B **50** (1994) 9300.
 - [10] M. Giovannini, I. Čurlík, F. Gastaldo, M. Reiffers, J. G. Sereni, *The role of crystal chemistry in $\text{YbCu}_{5-x}\text{Au}_x$* , J. Alloys Compd. **627**, 2024 (2015).
 - [11] I. Čurlík, M. Reiffers, and M. Giovannini, *Study of magnetic contribution to the heat capacity of YbCu_4Ni* , Acta Phys. Polonica A **122**, 3 (2012).
 - [12] J. He, G. Ling, Z. Jia, *Magnetic and transport properties of cubic AuBe_5 -type $\text{YbCu}_{5-x}\text{Ga}_x$ system*, Physica B: Condensed Matter **301** (2001) 196-202.
 - [13] J. Banda, D. Hafner, J.F. Landacta, E. Hassinger, K. Mutsimoto, M. Giovannini, J.G. Sereni, C. Geibel, M. Brando; *Electronuclear Quantum Criticality*, arXiv:2308.15294 [cond-mat.str-el] 29 Aug 2023.
 - [14] I. Čurlík, M. Reiffers, J.G. Sereni, M. Giovannini, S. Gabani, *Searching for a quantum critical point in $\text{YbCu}_{5-x}\text{Au}_x$* , arXiv: 1403.6004 [cond-mat.str-el] March 2014.
 - [15] J.G. Sereni; *Thermodynamic analysis of the quantum critical behavior of Ce-lattice compounds*; Phil. Mag. **93** (2013) 409.
 - [16] J.G. Sereni; *The effect of the electronic and structural environment on the valence of Ce*, J. Less Common Metals, **86** 287-298 (1982).
 - [17] A. Tari, *The Specific Heat of Matter at Low Temperature*, Imperial College Press, 2003.
 - [18] X. Zhang, Te Zhang, Z. Zhuang, Z. Leng, Z. Wei, X. Liu, J. Xiang, S. Zhang, P. Sun; *YbNi_4Mg : Superheavy fermion with enhanced Wilson ratio and magnetocaloric effect*; Phys. Rev. M **9** (2025) 014402.
 - [19] G. R. Stewart, Rev. Mod. Phys. **73** (2001) 797.
 - [20] J.G. Sereni, C. Geibel, M.G-Berisso, P. Hellmann, O. Trovrelli, F. Steglich, *Scaling of the " $C_p \propto T \ln T$ " dependence in Ce systems*, Physica B **230** (1997) 580 and references therein.
 - [21] H.v. Löhneysen, M. Sieck, O. Stockert, M. Waffenschmidt; *Investigation of non-Fermi-liquid behavior in $\text{CeCu}_{6-x}\text{Au}_{1-x}$* ; Physica B **223&224** (1996) 471-774.
 - [22] F. Steglich, P. Gegenwart, C. Geibel, R. Helfrich, P. Hellmann, M. Lang, A. Link, R. Modler, G. Sparn, N. Büttgen, A. Loidl; *New observations concerning magnetism and superconductivity in heavy-fermion metals*; Physica B: Condensed Matter **223 & 224** (1996) 1-8.
 - [23] Y. Tokiwa, B. Piening, H. S. Jeevan, S. L. Bud'ko, P.C. Canfield, P. Gegenwart; *Super-heavy electron material as metallic refrigerant for adiabatic demagnetization cooling*; Sci. Adv. **2** (2016) e1600835.
 - [24] F. Akbar, I. Čurlík, M. Reiffers, M. Giovannini; *Phase equilibria and crystal structures in the ytterbium-copper-zinc system*, Jour. of Alloys and Compounds **976** (2024) 173195.
 - [25] A.A. Katanin, *Extracting Kondo temperature of strongly- correlated systems from the inverse local magnetic susceptibility*, Nat. Comm. **12** (2021) 1433.
 - [26] See for example: <https://www.webelements.com/ytterbium/isotopes>.
 - [27] J.-M Mignot, *Interactions hyperfines et effect Kondo dans les alliages AuYb* , PhD Thesis, University of Grenoble, March 1980.
 - [28] See for example: S. Blundell; *Magnetism in Condensed Matter*, Oxford, University Press (N.Y.), 2001.
 - [29] H. Rudigier, H.R. Ott, O. Vogt; *Low temperature specific heat of uranium mononictides and monochalcogenides*; Phys. Rev. B **32** (1985) 4584.
 - [30] L.J. Tao, D. Davidov, R. Orbach E.P. Chock; *Hyperfine Splitting of Er and Yb Resonances in Au*; Phys. Rev. B **4** (1971) 5.